Science Advances
AAAS

Supplementary Materials for

Structures of neurokinin 1 receptor in complex with G_q and G_s proteins reveal substance P binding mode and unique activation features

Cristian Thom, Janosch Ehrenmann, Santiago Vacca, Yann Waltenspühl, Jendrik Schöppe, Ohad Medalia, Andreas Plückthun*

*Corresponding author. Email: plueckthun@bioc.uzh.ch

Published 8 December 2021, *Sci. Adv.* **7**, eabk2872 (2021)
DOI: 10.1126/sciadv.abk2872

This PDF file includes:

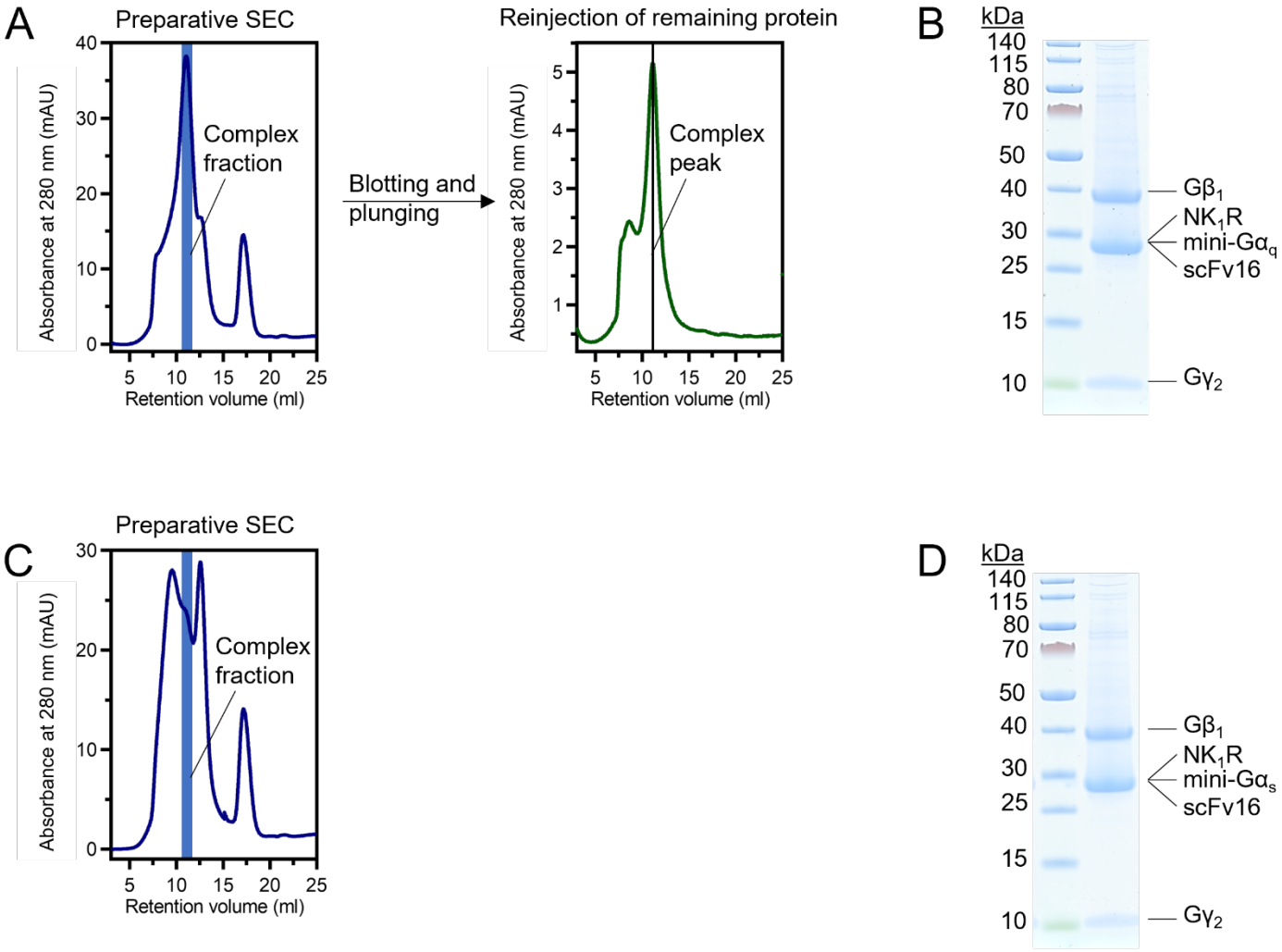

Fig. S1. NK_1R complexes: SEC and LDS-PAGE.
(A) SEC of the NK_1R:G_q complex. Left: Preparative SEC profile with the collected complex fraction indicated by a blue bar. Right: Analytical SEC profile of the remaining protein (concentrated collected complex fraction) after blotting and plunging (~3 h after fraction collection). Retention volume of the complex: 11.1 ml.
(B) LDS-PAGE gel of the NK_1R:G_q complex with complex components indicated. NK_1R, mini-$G\alpha_q$, and scFv16 run at the same apparent molecular weight (confirmed by LDS-PAGE of the individual components, gel not shown).
(C) Preparative SEC profile of the NK_1R:G_s complex with the collected complex fraction indicated by a blue bar. After blotting and plunging no sufficient quantity of protein for analytical SEC remained.
(D) LDS-PAGE gel of the NK_1R:G_s complex with complex components indicated. NK_1R, mini-$G\alpha_s$, and scFv16 run at the same apparent molecular weight (confirmed by LDS-PAGE of the individual components, gel not shown).

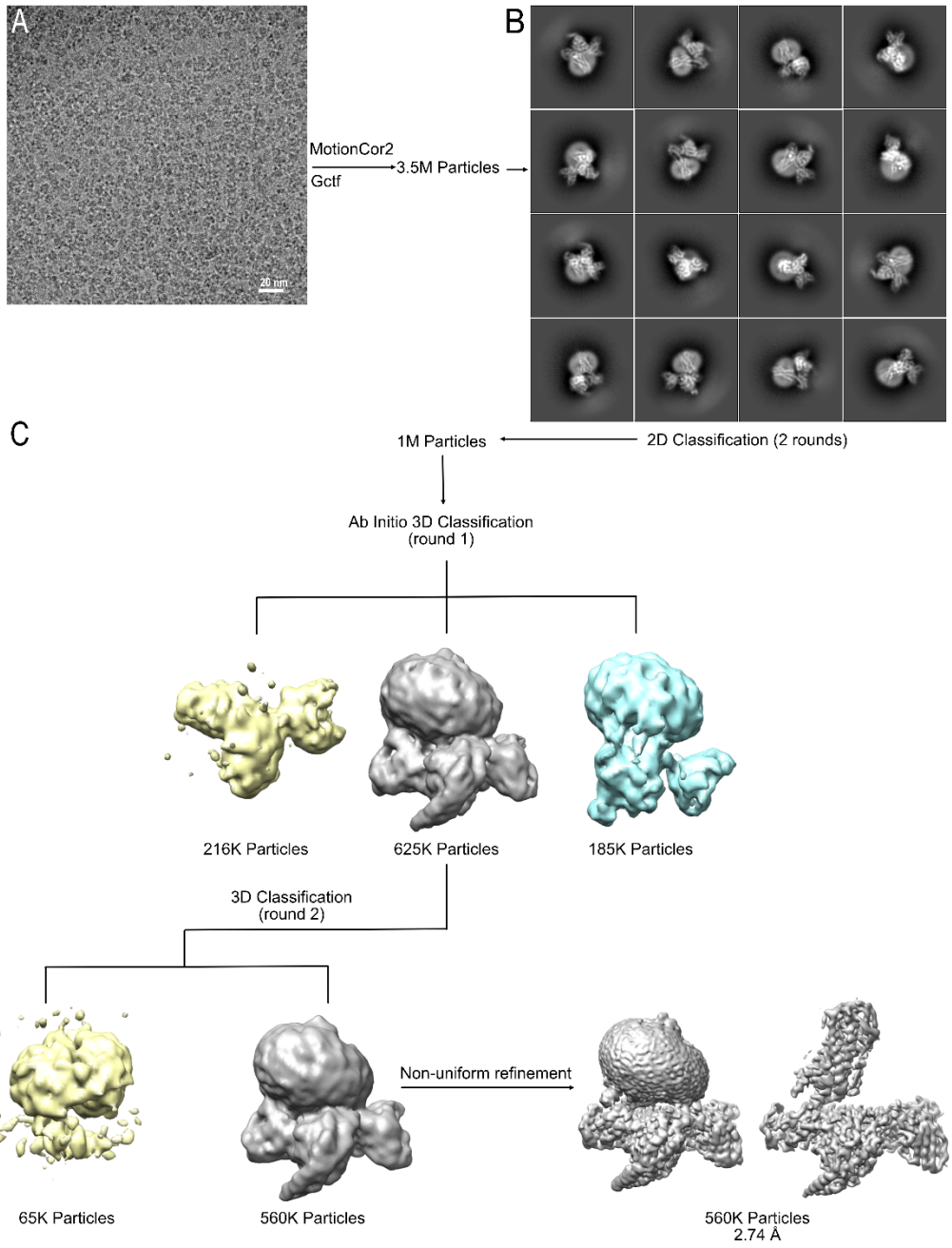

Fig. S2. Workflow for cryo-EM data processing of the NK_1R:SP:G_q:scFv16 complex.
(A) Representative cryo-EM micrograph of the NK_1R:SP:G_q:scFv16 complex. Scale bar, 20 nm.
(B) Representative 2D averages showing distinct secondary structure features from different views of the complex after 2 rounds of 2D classification.
(C) 3D classification workflow and refinement.

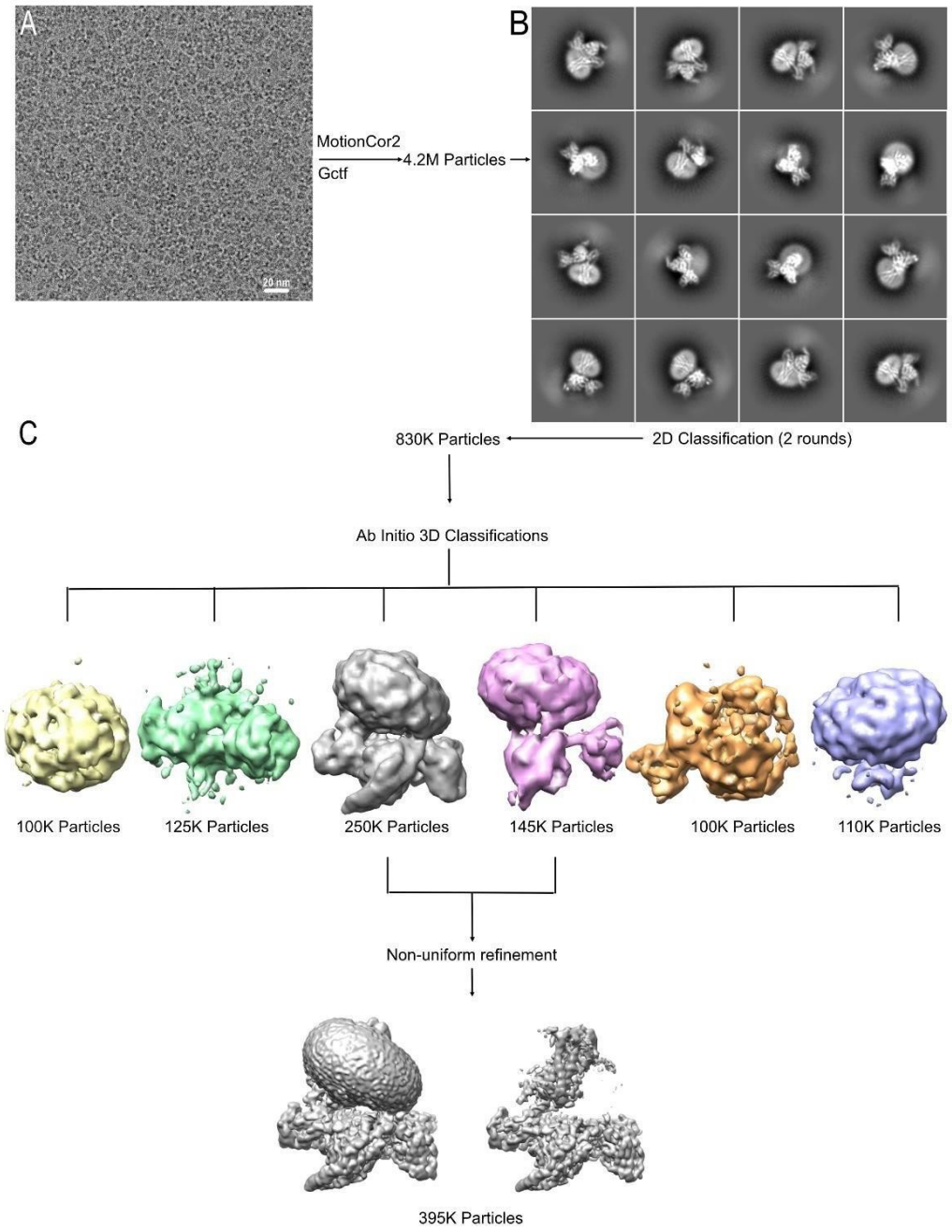

Fig. S3. Workflow for cryo-EM data processing of the NK_1R:SP:G_s:scFv16 complex.
(A) Representative cryo-EM micrograph of the NK_1R:SP:G_s:scFv16 complex. Scale bar, 20 nm.
(B) Representative 2D averages showing distinct secondary structure features from different views of the complex after 2 rounds of 2D-classification.
(C) 3D classification workflow and refinement.

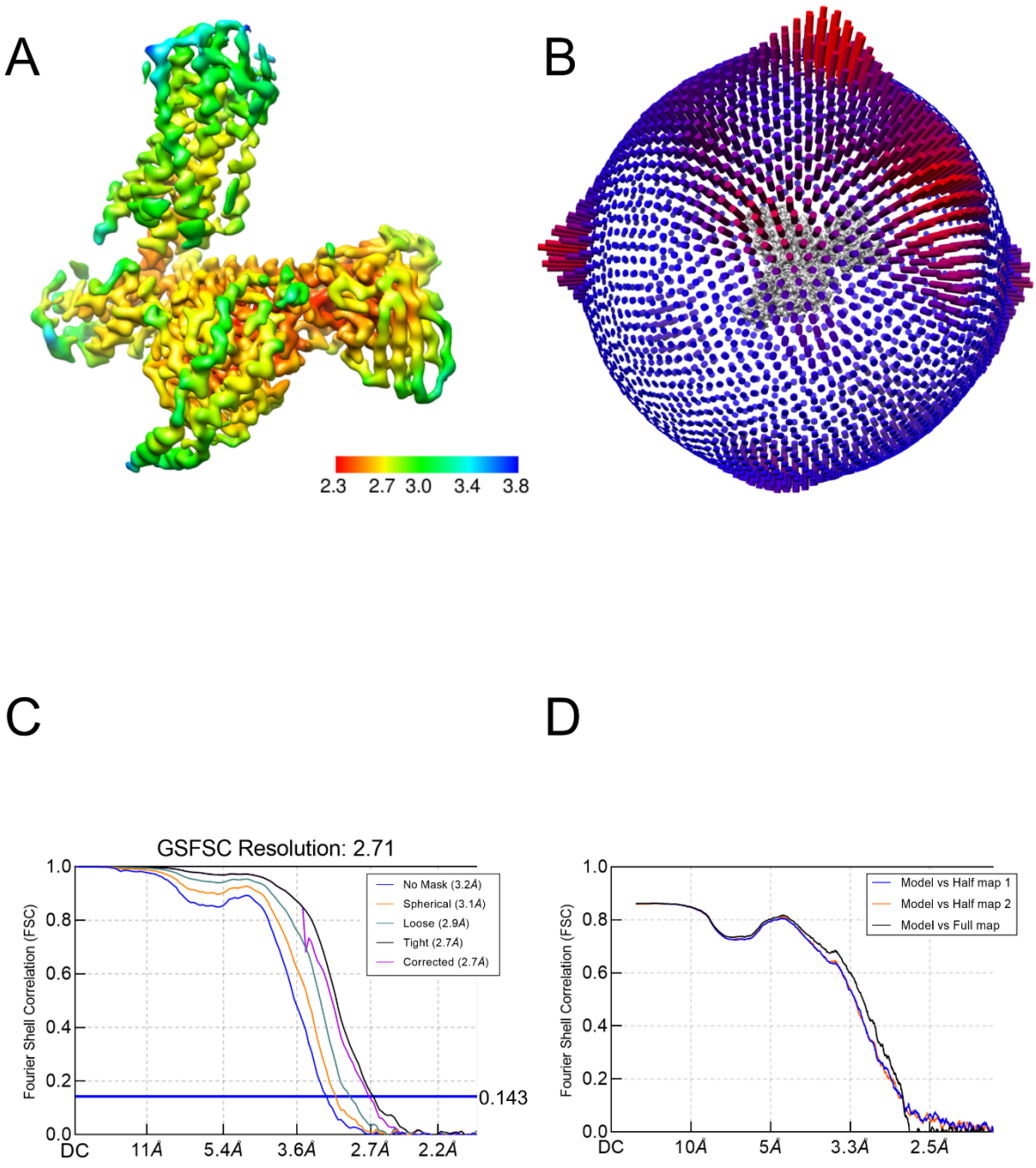

Fig. S4. Resolution of the NK$_1$R:SP:G$_q$:scFv16 complex.
(A) Local resolution analysis of the NK$_1$R:SP:G$_q$:scFv16 complex.
(B) Angular distribution of the particle orientations of the NK$_1$R:SP:G$_q$:scFv16 complex.
(C) The gold-standard Fourier shell correlation curves for the map of the NK$_1$R:SP:G$_q$:scFv16 complex.
(D) For cross validation, FSC curves of the refined model versus full map (black), refined map versus half map 1 (blue), and refined model versus half map 2 (orange) were calculated.

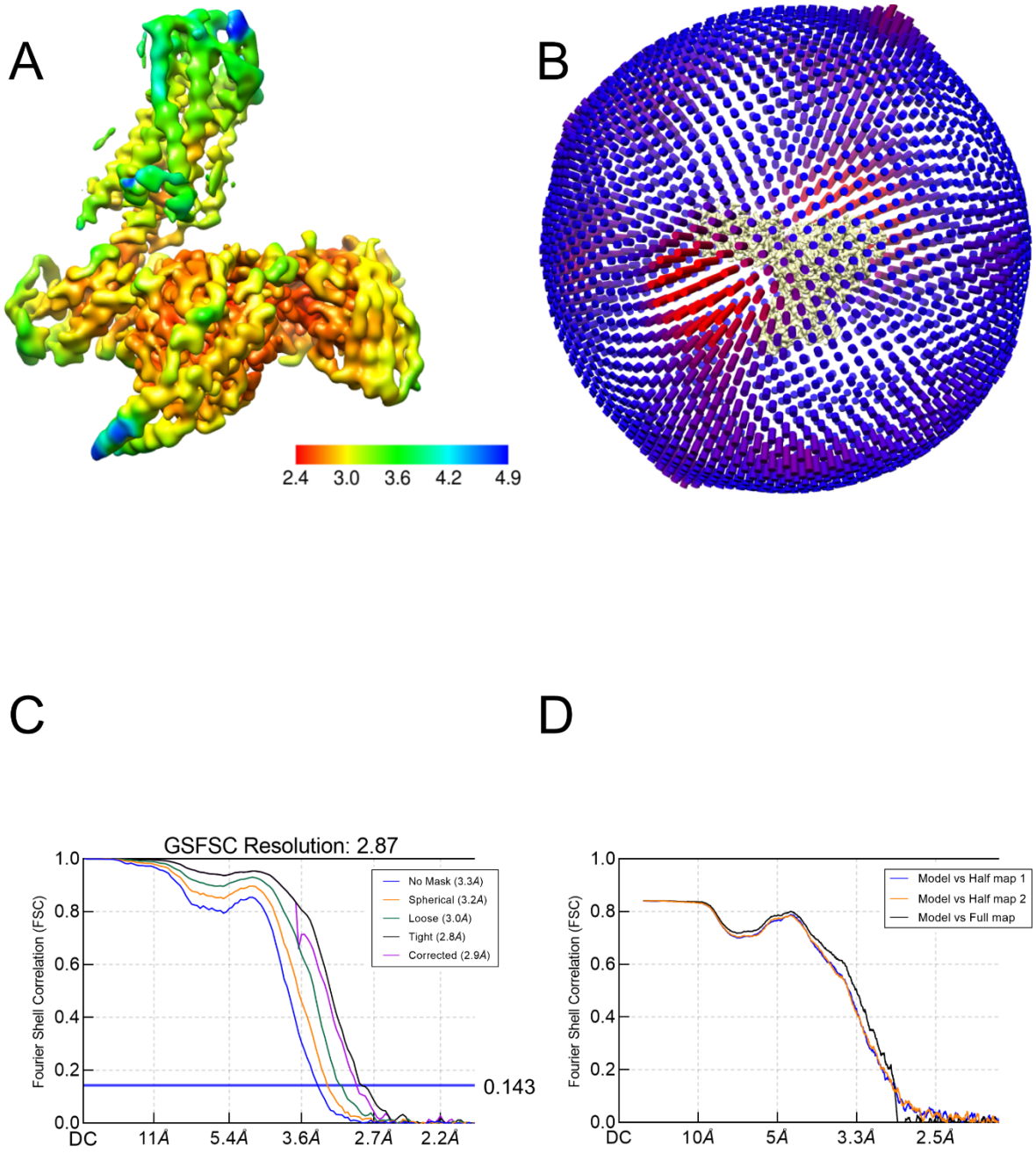

Fig. S5. Resolution of the NK_1R:SP:G_s:scFv16 complex.
(A) Local resolution analysis of the NK_1R:SP:G_s:scFv16 complex.
(B) Angular distribution of the particle orientations of the NK_1R:SP:G_s:scFv16 complex.
(C) The gold-standard Fourier shell correlation curves for the map of the NK_1R:SP:G_s:scFv16 complex.
(D) For cross validation, FSC curves of the refined model versus full map (black), refined map versus half map 1 (blue), and refined model versus half map 2 (orange) were calculated.

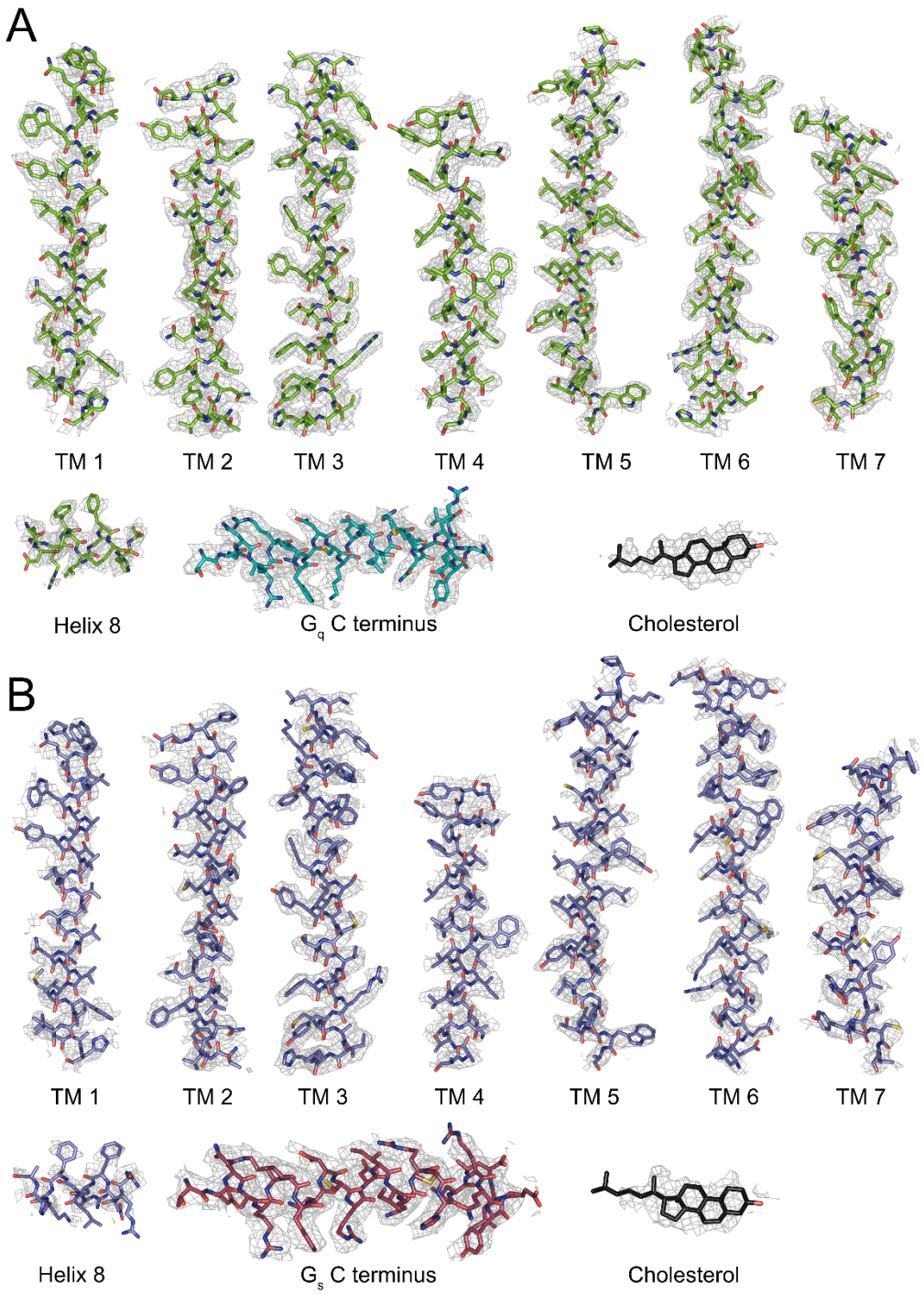

Fig. S6. Cryo-EM density within NK_1R.
(A) Cryo-EM density maps are shown for $G\alpha_q$ Cα5 helix, cholesterol, NK_1R helix 8, and all seven transmembrane α-helices of the NK_1R:G_q complex.
(B) Cryo-EM density maps are shown for $G\alpha_s$ Cα5 helix, cholesterol, NK_1R helix 8, and all seven transmembrane α-helices of the NK_1R:G_s complex.

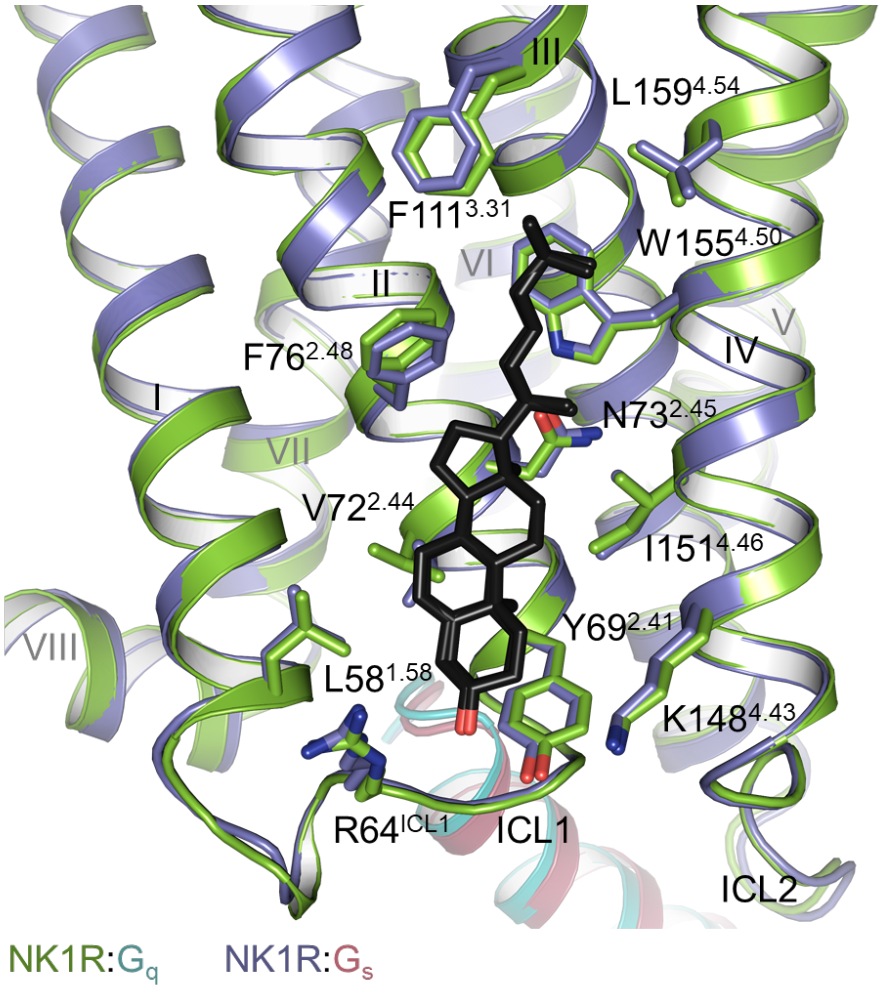

Fig. S7. Cholesterol binding site in NK_1R.
Structural superposition of NK_1R:G_q and NK_1R:G_s with cholesterol shown in black. Residues within 4 Å distance of cholesterol are depicted as sticks.

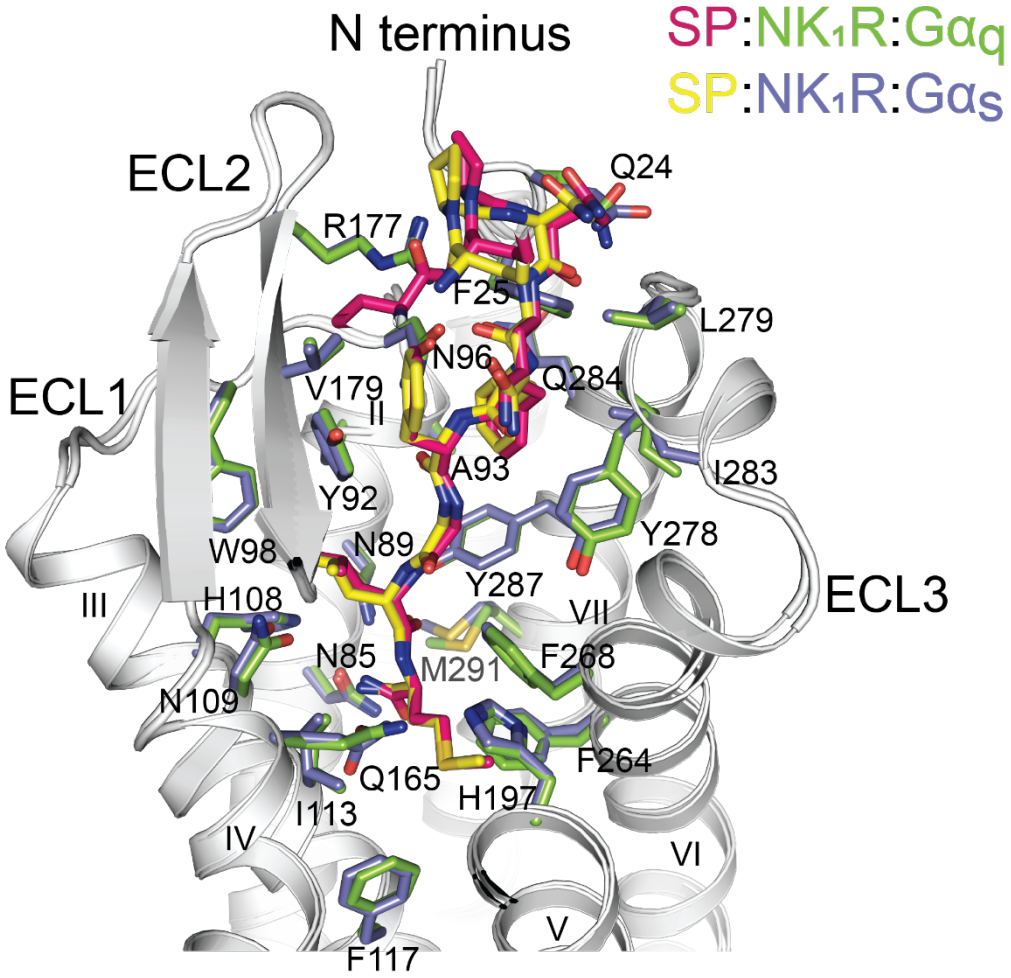

Fig. S8. Structural superposition of the orthosteric SP binding pocket in $NK_1R:G_q$ and $NK_1R:G_s$.

SP and SP-interacting NK_1R residues are shown as sticks in the respective color scheme of the complex.

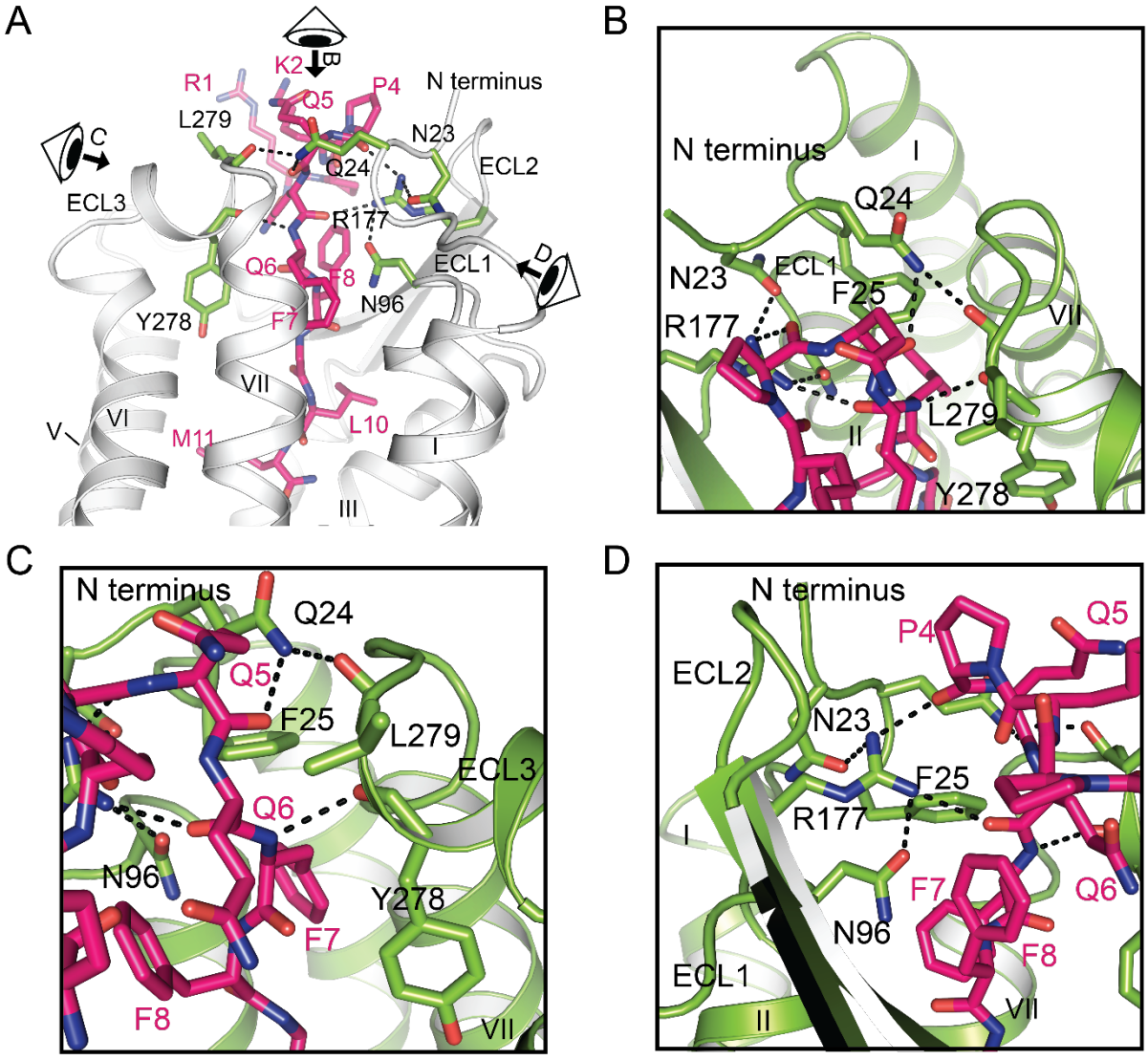

Fig. S9. Close-up views on the extracellular hydrogen-bonding network established by SP.

(A) Overview as in Fig. 2F with points of view for (B-D) indicated.

(B to D) Close-up views on the extracellular hydrogen-bonding network.

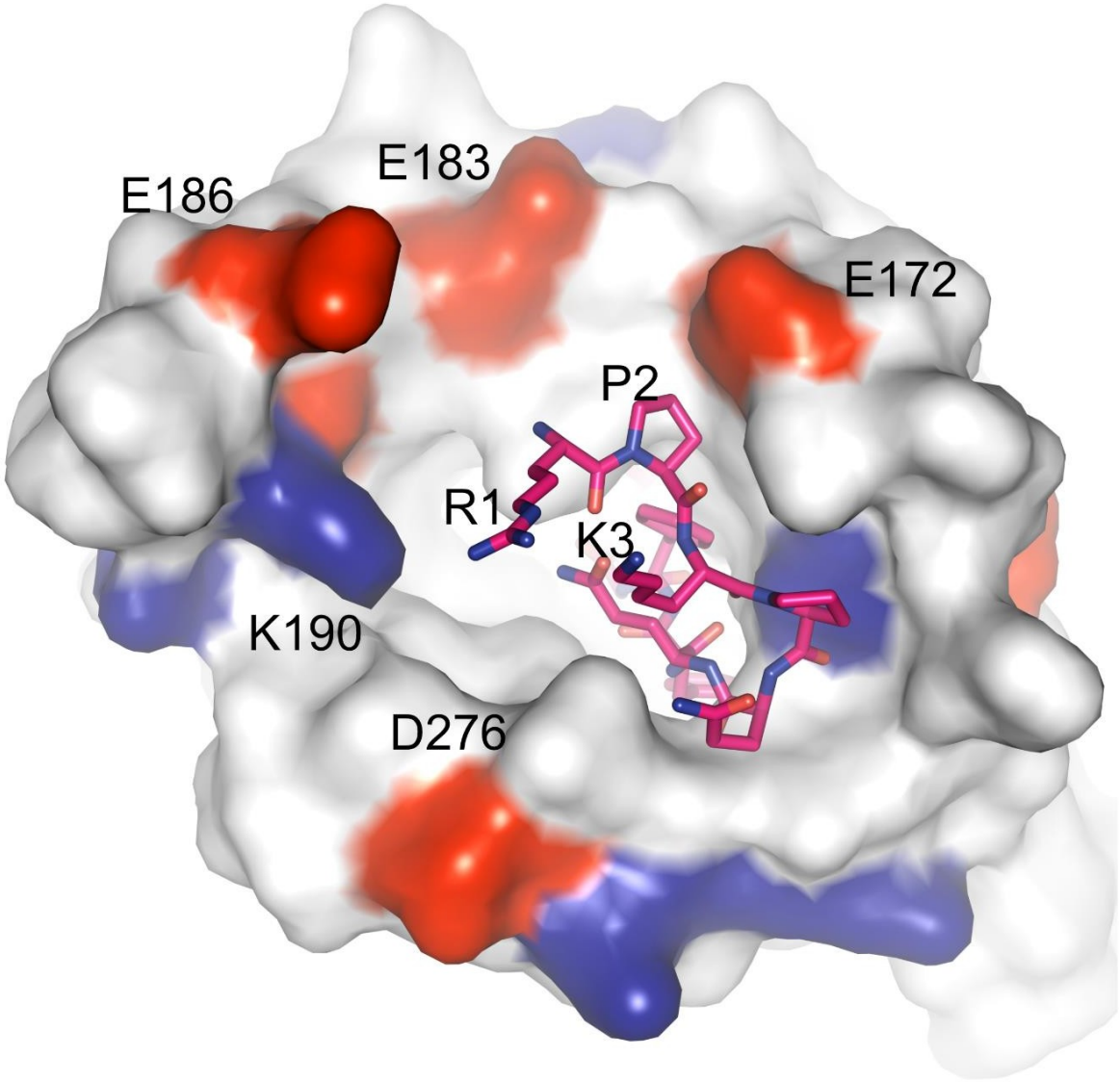

Fig. S10. Charge distribution on the extracellular surface of NK_1R.
Extracellular view of a surface representation of the NK_1R:SP complex with negatively charged residues in red (amino acids D and E), and positively charged residues in blue (amino acids R and K).

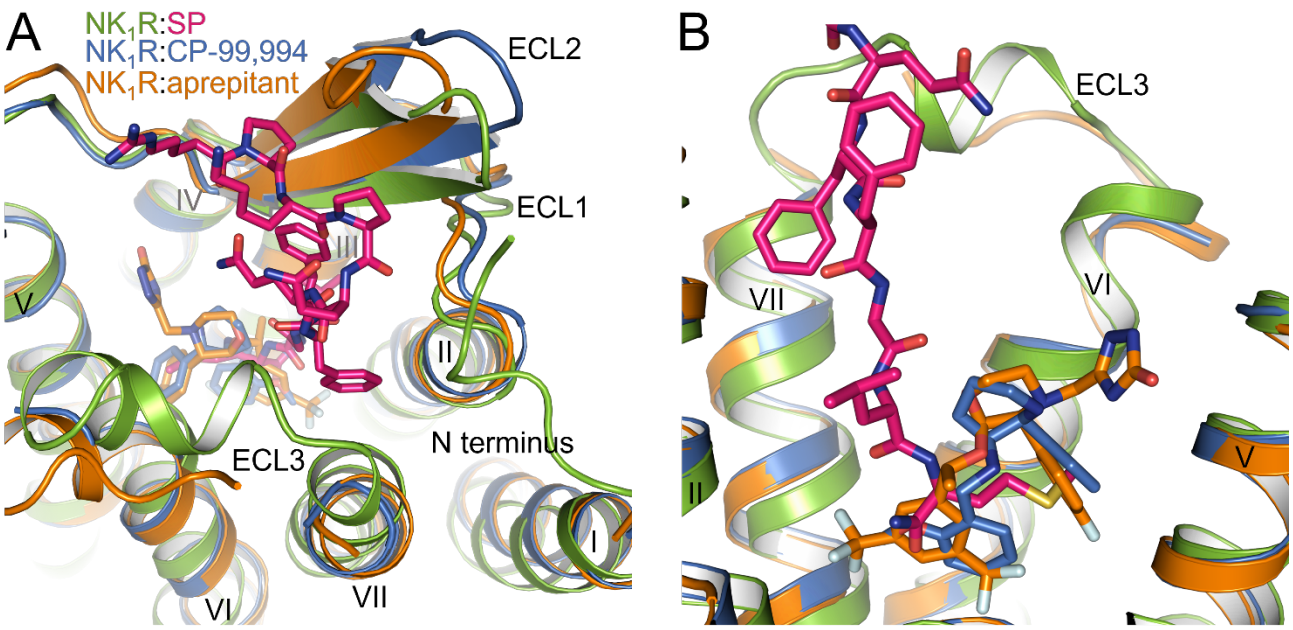

Fig. S11. Comparison of NK_1R:SP, NK_1R:CP-99,994 and NK_1R:aprepitant.
(A) Superposition of NK_1R:SP (G_q complex), NK_1R:CP-99,994 (PDB ID: 6HLL), and NK_1R:aprepitant (PDB ID: 6HLO) as viewed from the extracellular space.
(B) Close-up view on the ligands bound in the orthosteric pocket.

Table S1. Ligand binding data to NK_1R with single amino acid mutations

construct	K_D [nM]	fold change (to wt)	ΔpK_D (to wt)	B_{max} (%wt)	surface expression (%wt)	n
NK_1R (wt)	7 ± 1					19
N23A	124 ± 17	17.6 ± 2.4	-1.23 ± 0.06	88 ± 8	135 ± 12	5
N23Q	52 ± 5	7.3 ± 0.6	-0.86 ± 0.04	102 ± 7	151 ± 18	4
Q24A	52 ± 6	7.4 ± 0.8	-0.86 ± 0.05	101 ± 9	103 ± 14	4
Q24N	35 ± 2	5.0 ± 0.3	-0.70 ± 0.02	115 ± 9	154 ± 24	4
F25A	109 ± 47	15.5 ± 6.6	-1.02 ± 0.23	18 ± 3	87 ± 13	4
F25Y	11 ± 3	1.6 ± 0.4	-0.14 ± 0.12	72 ± 15	79 ± 29	4
N85A	59 ± 5	8.3 ± 0.7	-0.92 ± 0.04	89 ± 5	125 ± 6	3
N85D	71 ± 19	10.1 ± 2.7	-0.96 ± 0.12	65 ± 4	85 ± 8	4
N85Q	72 ± 26	10.3 ± 3.6	-0.87 ± 0.16	57 ± 6	86 ± 5	6
N89A	251 ± 38	35.7 ± 5.4	-1.54 ± 0.06	111 ± 14	163 ± 25	3
N89D	485 ± 211	69.0 ± 30.0	-1.56 ± 0.29	64 ± 21	120 ± 5	5
N89Q	782 ± 222	111.2 ± 31.6	-2.00 ± 0.10	110 ± 27	125 ± 6	4
Y92A	76 ± 5	10.8 ± 0.8	-1.03 ± 0.03	54 ± 5	74 ± 7	3
Y92F	8 ± 2	1.1 ± 0.2	-0.02 ± 0.09	62 ± 4	87 ± 5	3
N96A	62 ± 9	8.9 ± 1.3	-0.94 ± 0.06	78 ± 8	99 ± 12	3
N96D	15 ± 2	2.2 ± 0.3	-0.33 ± 0.05	86 ± 3	122 ± 11	3
N96Q	108 ± 8	15.4 ± 1.2	-1.19 ± 0.03	107 ± 4	133 ± 19	3
F117A	66 ± 10	9.4 ± 1.4	-0.96 ± 0.06	123 ± 5	111 ± 15	3
Q165A	77 ± 13	10.9 ± 1.9	-1.02 ± 0.08	106 ± 1	171 ± 45	3
R177A	321 ± 143	45.7 ± 20.4	-1.47 ± 0.18	56 ± 4	88 ± 9	6
R177K	419 ± 20	59.6 ± 2.9	-1.77 ± 0.02	87 ± 4	96 ± 9	4
V179A	64 ± 10	9.2 ± 1.4	-0.94 ± 0.07	86 ± 3	103 ± 10	5
F264A	32 ± 4	4.5 ± 0.6	-0.65 ± 0.06	89 ± 10	142 ± 26	3
F268A	195 ± 20	27.7 ± 2.9	-1.44 ± 0.04	138 ± 19	216 ± 36	3
Y278A	17 ± 5	2.4 ± 0.7	-0.33 ± 0.10	111 ± 6	140 ± 21	4
I283A	115 ± 21	16.4 ± 3.0	-1.19 ± 0.07	99 ± 6	137 ± 29	5
Q284A	93 ± 17	13.3 ± 2.4	-1.10 ± 0.07	74 ± 7	109 ± 17	4
Y287A	218 ± 140	31.0 ± 19.9	-1.30 ± 0.28	29 ± 14	60 ± 11	3
M291A	43 ± 12	6.1 ± 1.7	-0.69 ± 0.19	57 ± 3	85 ± 10	4

Whole-cell specific saturation binding experiment of fluorescently labelled peptide SP-HL488 to HEK293T cells expressing wild-type and mutated NK_1R variants. Binding curves were analyzed by global fitting to a one-site saturation binding equation. All values are expressed as mean ± SEM of the indicated number of independent experiments performed in duplicate. Cell surface expression was obtained by measuring fluorescence emission of SNAP-Lumi4-Tb-labeled receptors.

Table S2. List of contacts between NK_1R and $G\alpha_s$

$G\alpha_s$ residue	$G\alpha_s$ portion	NK_1R residue	NK_1R portion	Type of interaction
R31$^{hns1.02}$	hns1 loop	R141^{ICL2}	ICL2	Hydrogen bond with peptide backbone
		S143$^{4.38}$	IV	Hydrogen bond
H34$^{S1.02}$	S1 loop	L138^{ICL2}	ICL2	Hydrogen bond with peptide backbone / Nonbonded contact
V210$^{S3.01}$	S3 loop	L138^{ICL2}	ICL2	Nonbonded contact
		Q139^{ICL2}	ICL2	Nonbonded contact
F212$^{S3.03}$		L138^{ICL2}	ICL2	Nonbonded contact
F359$^{H5.08}$	Cα5	L138^{ICL2}	ICL2	Nonbonded contact
C362$^{H5.11}$	Cα5	L138^{ICL2}	ICL2	Nonbonded contact
R363$^{H5.12}$	Cα5	I135$^{3.55}$	III	Hydrogen bond with peptide backbone
		P137^{ICL2}	ICL2	Nonbonded contact
		L138^{ICL2}	ICL2	Nonbonded contact
I366$^{H5.15}$	Cα5	P137^{ICL2}	ICL2	Nonbonded contact
		L138^{ICL2}	ICL2	Nonbonded contact
Q367$^{H5.16}$	Cα5	I134$^{3.54}$	III	Hydrogen bond with peptide backbone / Nonbonded contact
		P137^{ICL2}	ICL2	Nonbonded contact
		L223$^{5.65}$	V	Nonbonded contact
R368$^{H5.17}$	Cα5	Q239$^{6.26}$	VI	Nonbonded contact
H370$^{H5.19}$	Cα5	A133$^{3.53}$	III	Nonbonded contact
		P137^{ICL2}	ICL2	Hydrogen bond with peptide backbone
Q373$^{H5.22}$	Cα5	T67$^{2.39}$	II	Hydrogen bond
Y374$^{H5.23}$	Cα5	T67$^{2.39}$	II	Nonbonded contact
		D129$^{3.49}$	III	Nonbonded contact
		A133$^{3.53}$	III	Nonbonded contact
		R141^{ICL2}	ICL2	Nonbonded contact
L376$^{H5.25}$	Cα5	R130$^{3.50}$	III	Nonbonded contact
		I134$^{3.54}$	III	Nonbonded contact
		V246$^{6.33}$	VI	Nonbonded contact
		M249$^{6.36}$	VI	Nonbonded contact
		L308$^{7.56}$	VII	Nonbonded contact
L377$^{H5.26}$	Cα5	A242$^{6.29}$	VI	Nonbonded contact
		V246$^{6.33}$	VI	Nonbonded contact
		L308$^{7.56}$	VII	Hydrogen bond with peptide backbone
		N309$^{8.47}$	VIII	Hydrogen bond with peptide backbone

Table S3. List of contacts between NK_1R and $G\alpha_q$

$G\alpha_q$ residue	$G\alpha_q$ portion	NK_1R residue	NK_1R portion	Type of interaction
R31$^{hns1.02}$	hns1 loop	R141^{ICL2}	ICL2	Hydrogen bond with peptide backbone
		S143$^{4.38}$	IV	Hydrogen bond
H34$^{S1.02}$	S1 loop	L138^{ICL2}	ICL2	Hydrogen bond with peptide backbone / Nonbonded contact
V210$^{S3.01}$	S3 loop	L138^{ICL2}	ICL2	Nonbonded contact
		Q139$^{6.26}$	VI	Nonbonded contact
F212$^{S3.03}$	S3 loop	L138^{ICL2}	ICL2	Nonbonded contact
F359$^{H5.08}$	Cα5	L138^{ICL2}	ICL2	Nonbonded contact
C362$^{H5.11}$	Cα5	L138^{ICL2}	ICL2	Nonbonded contact
K363$^{H5.12}$	Cα5	P137^{ICL2}	ICL2	Nonbonded contact
		L138^{ICL2}	ICL2	Nonbonded contact
I366$^{H5.15}$	Cα5	P137^{ICL2}	ICL2	Nonbonded contact
		L138^{ICL2}	ICL2	Nonbonded contact
L367$^{H5.16}$	Cα5	I134$^{3.54}$	III	Nonbonded contact
Q368$^{H5.17}$	Cα5	Q239$^{6.26}$	VI	Hydrogen bond
N370$^{H5.19}$	Cα5	A133$^{3.53}$	III	Hydrogen bond to peptide backbone
E373 $^{H5.22}$	Cα5	T67$^{2.39}$	II	Hydrogen bond / Nonbonded contact
Y374$^{H5.23}$	Cα5	T67$^{2.39}$	II	Nonbonded contact
		D129$^{3.49}$	III	Nonbonded contact
		A133$^{3.53}$	III	Nonbonded contact
		R141^{ICL2}	ICL2	Nonbonded contact
N375$^{H5.24}$	Cα5	N68$^{2.40}$	II	Hydrogen bond
		L71$^{2.43}$	II	Nonbonded contact
		N309$^{8.47}$	VIII	Hydrogen bond
		F312$^{8.50}$	VIII	Nonbonded contact
L376$^{H5.25}$	Cα5	R130$^{3.50}$	III	Nonbonded contact
		I134$^{3.54}$	III	Nonbonded contact
		V246$^{6.33}$	VI	Nonbonded contact
		M249$^{6.36}$	VI	Nonbonded contact
		L308$^{7.56}$	VII	Nonbonded contact
V377$^{H5.26}$	Cα5	A242$^{6.29}$	VI	Nonbonded contact
		V246$^{6.33}$	VI	Nonbonded contact
		L308$^{7.56}$	VII	Hydrogen bond with peptide backbone
		N309$^{8.47}$	VIII	Hydrogen bond with peptide backbone